RESEARCH ARTICLE

Macromolecular Materials and Engineering
Open Access
www.mame-journal.de

In Vitro Neuroprotective Effect Evaluation of Donepezil-Loaded PLGA Nanoparticles-Embedded PVA/PEG Nanofibers on SH-SY5Y Cells and AP-APP Plasmid Related Alzheimer Cell Line Model

Ece Guler, Humeyra Betul Yekeler, Burcu Uner, Murat Dogan, Asima Asghar, Fakhera Ikram, Yusufhan Yazir, Oguzhan Gunduz, Deepak M Kalaskar, and Muhammet Emin Cam**

Recently developed nanoparticles and nanofibers present new brain-specific treatment strategies, especially for Alzheimer's disease treatment. In this study, donepezil (DO)-loaded PLGA nanoparticles (DNP) are embedded in PVA/PEG nanofibers (DNPF) produced by pressurized gyration for sublingual administration. SEM images showed produced drug-loaded and pure nanofibers, which have sizes between 978 and 1123 nm, demonstrated beadless morphology and homogeneous distribution. FT-IR, XRD, and DSC results proved the produced nanoparticles and fibers to consist of the DO and other polymers. The in vitro drug release test presented that the release profile of DO is completed at the end of the 18th day. It is released by the first order kinetic model. DNPF has an ultra-fast release profile via its disintegration within 2 sec, which proved itself to be suitable for the administration sublingually. All samples presented above ≈90% cell viability via their non-toxic natures on SH-SY5Y human neuroblastoma cells by using Alamar blue assay. The anti-Alzheimer effects of DO, DNP, and DNPF are evaluated on the Aβ_{1-42}-induced SH-SY5Y cells at 1, 5, and 10 µM as treatment groups. The 1 µM dosage exhibited the most significant neuroprotective effects, which showed enhanced cellular uptake and superior modulation of Alzheimer's-related proteins, including tau and Aβ.

1. Introduction

Alzheimer's disease (AD) is a highly prevalent neurodegenerative form of dementia. This disease is identified by cognitive dysfunctions, namely executive problems, impairment of expressive speech, and visuospatial abnormalities. Furthermore, pathological evidence of apathy and agitation caused by existing AD presents that these symptoms are associated with the degeneration in cholinergic neuron–rich regions, especially the anterior cingulate cortex, posterior cingulate cortex, nucleus basalis of Meynert, and frontal cortex. These cognitive dysfunctions cause impaired independence, decreased quality of a patient's life, serious socio-economic problems, and, as a result, addicted daily life to someone. Dementia-related to AD exhibits gradual onset and prominent progressive amnestic symptoms.[1,2]
AD, which affects over 50 million people worldwide, is sourced by a combination of

E. Guler, M. E. Cam
Department of Pharmacology, School of Pharmacy
Istanbul Kent University
Istanbul 34406, Kagithane, Türkiye
E-mail: m.cam@ucl.ac.uk

E. Guler, H. B. Yekeler, O. Gunduz
Center for Nanotechnology and Biomaterials Application and Research
Marmara University
Istanbul 34722, Türkiye

E. Guler, H. B. Yekeler, D. M Kalaskar, M. E. Cam
UCL Division of Surgery and Interventional Sciences
Rowland Hill Street, London NW3 2PF, UK
E-mail: d.kalaskar@ucl.ac.uk

E. Guler, H. B. Yekeler, B. Uner, M. E. Cam
MecNano Technologies
Cube Incubation
Istanbul 34906, Teknopark İstanbul, Türkiye

H. B. Yekeler
Department of Pharmacology, Faculty of Pharmacy
Marmara University
Istanbul 34854, Türkiye

The ORCID identification number(s) for the author(s) of this article can be found under https://doi.org/10.1002/mame.202400160

DOI: 10.1002/mame.202400160

factors affecting the brain over time, such as lifestyle, environmental factors, and genetics. Neuroinflammation, irreversible neuron loss, amyloid plaque accumulation, neurofibrillary tangles derived from tau hyperphosphorylation, and transmission deficiency cause the formation of AD pathology in the brain.[1,3,4] Nowadays, galantamine, donepezil (DO), and rivastigmine have been approved as reversible acetylcholinesterase inhibitors (AChEI) by the European Medicines Agency (EMA) and the U.S. Food and Drug Administration (FDA) for the improvement of patient life quality in the AD treatment.[5–7]

DO, which is a specific reversible AChEI, is preferred to increase the concentration of acetylcholine and protect AD patients' brains from neuroinflammation. Nowadays, DO is applied as an oral formulation (5–10 mg). However, the oral administration of DO causes various gastrointestinal side effects such as diarrhea or nausea. In addition, the blood-brain barrier (BBB) poses a limitation to the delivery of hydrophilic DO to the brain. This barrier impedes the passage of drugs to the brain in high concentration. Thus, the improvement of an effective alternative treatment strategy is required to help mask the hydrophilic nature of DO and increase the DO concentration in the AD patient's brain.[8,9]

B. Uner
Department of Pharmaceutical Technology, School of Pharmacy
Istanbul Kent University
Istanbul 34406, Türkiye

B. Uner
Department of Pharmaceutical and Administrative Science
University of Health Science and Pharmacy in St. Louis
St. Louis 63110, MO, USA

B. Uner
Department of Anesthesiology
Center for Clinical Pharmacology
Washington University School of Medicine in St. Louis
St. Louis 63110, MO, USA

M. Dogan
Department of Pharmaceutical Biotechnology
Faculty of Pharmacy
Sivas Cumhuriyet University
Sivas 58140, Türkiye

M. Dogan
Cancer Survivorship Institute
Robert H. Lurie Comprehensive Cancer Center
Northwestern University
625 N. Michigan Ave., Suite 2100, Chicago 60611, IL, USA

A. Asghar, F. Ikram
Interdisciplinary Research Centre in Biomedical Materials
COMSATS University Islamabad
Lahore Campus, Pakistan

Y. Yazir
Stem Cell and Gene Therapies Research and Applied Center, Medical Faculty
Kocaeli University
Kocaeli 41380, Turkiye

O. Gunduz
Department of Metallurgical and Materials Engineering
Faculty of Technology
Marmara University
Istanbul 34730, Türkiye

M. E. Cam
Biomedical Engineering Department
University of Aveiro
Aveiro 3810-193, Portugal

Nanotechnology is a field of innovation and applied science, which includes various nano-sized drug delivery systems like nanoparticles, nanofibers, liposomes, dendrimers, nanoemulsions, metal-based carriers, etc. These nanopharmaceuticals present increased bioavailability, controlled and sustained drug release, and improved targeting properties to specific sites by modulating the lipophilicity, biodegradability, and hydrophilicity of drugs depending on their physicochemical characteristics. They have efficient roles in the passage of the blood-brain barrier (BBB) because their permeability is up to 200 nm.[10,11] Polylactic-co-glycolic acid (PLGA), which is synthesized by ring-opening co-polymerization of lactide and glycolide, exhibits biocompatibility and biodegradability properties approved by the FDA. However, PLGA nanoparticles have cleared fast from the reticuloendothelial system until reaching the brain. Thus, it is preferred to produce functionalized particles to enhance transport through the BBB. Polyethylene glycol (PEG), which is one of the hydrophilic polymers as a stabilizer, is chosen to attach the surfaces of PLGA nanoparticles to increase the surface hydrophilicity. The encapsulation of drugs in nanoparticles protects the drugs against environmental factors like gastric acid degradation, exhibits drugs to have prolonged half-life in the body, controlled and sustained release of drugs, and increased bioavailability. Furthermore, PEG-modified nanoparticles exhibit reduced protein adsorption and interaction with the mucus constituents, increased drug stability and particle translocation across the mucosa and mucus, enhanced delivery to lymph nodes, and prolonged systemic circulation due to lowered uptake by macrophages.[12–19]

Fibers in nanometers have high porosity, low density, good interconnectivity between the pores, larger surface area, and small pore size. They show controlled drug release and high drug-loading capacity. Nanofibers can be produced via different methods namely island-in-the-sea spinning, phase separation, melt blowing, template synthesis, molecular assembly, electrospinning, drawing, and pressurized gyration (PG).[20–22] In the PG process, the increased centrifugal force with enhanced rotational speed and occurred pressure differential because of the applied gas causes the polymer solution displacement. The fiber is produced from the extruded polymer that remains in the jet by the effect of solvent evaporation. It provides greater production rates and reduced power consumption in the fiber production process due to the advantages of the PG method.[23] Polyvinyl alcohol (PVA), which is a synthetic, semi-crystalline, water-soluble polymer, and non-ionic, has unique properties such as being biocompatible, chemically stable, non-hazardous, mechanically stable, inexpensive, and high electrical strength. Thus, it is one of the most preferred polymers in fiber production.[24,25] Loading the nanoparticle to nanofibers is one of the best options when prolonged drug release is targeted for the treatment of AD because of decreased patient compliance caused by memory loss in the usage of the drug. The initial burst release is seen in drug-loaded nanoparticles because of the adsorption of the drug during encapsulation or including weakly bound drugs. This situation is often irreproducible and uncontrollable. However, nanofibers exhibit diffusion-related drug release due to their core-sheath structure. Thus, nanoparticle-loaded nanofibers show decreased initial burst release, increased efficiency, and improved sustained release.[26,27]

The sublingual drug administration provides the drug rapid absorption, besides protecting it from the hepatic first-pass effect, gastric acid degradation, and entering the systemic circulation directly. The drug is exposed to limited enzymes and less mucin in saliva and it can be more stable, easily self-administer, and more beneficial for patients with swallowing difficulties.[19]

Herein, it was aimed to improve a new treatment strategy for patients with AD. DO-loaded PLGA nanoparticles (DNP) were embedded in PVA/PEG nanofibers (DNPF) produced by PG for sublingual administration. Therefore, it can target the brain, increasing bioavailability, providing sustained release, and enhancing the stability of DO. In addition, crystalline morphological, and chemical structures of all DNP and DNPF were evaluated by using X-ray diffraction (XRD), scanning electron microscopy (SEM), and Fourier transforms infrared spectroscopy (FT-IR), respectively. The physical parameters of the polymer blend and the thermal properties of the products were examined. Furthermore, in vitro drug release tests and wetting and disintegration tests were carried out. The cytotoxic and anti-Alzheimer's effects of DNP and DNPF were examined in the in vitro cell culture by using amyloid $\beta_{1\text{-}42}$ ($A\beta_{1\text{-}42}$)-induced SH-SY5Y human neuroblastoma cell line. To explore the mechanisms underlying these protein aggregates, we conducted an experiment to analyze the insoluble fractions of tau and $A\beta$ in human neural progenitor cells (HNPCs) following transfection with an amyloid precursor gene related amyloid beta precursor protein (AP-APP) plasmid. By fractionating and isolating these proteins, we were able to quantify their levels and assess their relevance to neurodegenerative processes using techniques such as Western blotting and real-time quantitative PCR. This study has implications for developing a novel drug delivery system with nanoparticles and nanofibers to improve the treatment of AD.

2. Results and Discussion

2.1. Physical Properties of Solutions, Morphology, Size Distribution of Fibers, and Zeta Potential of Nanoparticles

The produced nanofibers and nanoparticles were observed under the SEM in order to analyze their morphological structures. PVA/PEG nanofibers were produced in three different ratios 8:1, 9:1, and 10:1, respectively. The diameters of fibers decreased with increasing the ratio of PVA. For this reason, the PVA/PEG (10:1 v/v) ratio was chosen as the optimum ratio for loading DNP. The diameters of nanofibers increased after loading DNP from 978 ± 347 nm to 998 ± 297 nm. This increase is due to the loading of DNP on the surface of the nanofibers.[28] Furthermore, the sizes of PNP and DNP were determined as 289 ± 2 and 272 ± 2 nm, respectively. The morphological structures of nanoparticles were detected as uniform with standard dimensions and spherical. However, there was an aggregation between nanoparticles (**Figure 2**).

Zeta potential analysis was performed in order to measure the particle charges. The low zeta potential values of PNP and DNP were observed as 2.28 ± 0.05 and 2.24 ± 0.03 mV, respectively. It may be caused by the aggregation problem of the zeta potential to be under 30 mV.[29–31] Furthermore, to be under 0.5 of the polydispersity index (PDI) indicates a narrow particle size distribution.[32] This value was found as 0.306 ± 0.02 and 0.231 ± 0.02 for PNP and DNP, respectively. The reason for a decrease in the zeta potential is due to the negative charge acetate groups of PVA. However, since PVA causes a low zeta potential, it is expected to have a negative effect on the stability of the particle, but it reversed this situation with a steric shield [33] (**Table 1**).

Table 1. Zeta potential results of nanoparticles.

Samples	ζ potential [mV] ± SD	Size [nm] ± SD	PDI ± SD
DNP	2.24±0.03	272±2	0.231±0.02
PNP	2.28±0.05	289±2	0.306±0.02

All solution parameters like density, surface tension, and viscosity affect the production of homogeneous non-beaded nanofibers. Furthermore, these parameters have effects on the size of fibers. An increase in the viscosity of solutions causes them to produce fibers, which are more uniform and larger in fiber size [34,35]. Surface tension and density have effects on the fiber bead numbers due to their effects on the interaction between the polymer molecules and solutions of solvent. The bead number of fibers decreases as reducing surface tension and density [36]. In this study, the surface tension of the PVA/PEG solution decreased from 60.0 to 53.3 mN m^{-1} while the density and viscosity of the solution increased from 1.03 g mL^{-1} and 1740 mPa s to 1.08 g mL^{-1} and 2217 mPa s after loading DNP to this solution, respectively (**Figure 1**).

2.2. Fourier Transform Infrared Spectroscopy

Fourier transform infrared spectroscopy (FT-IR) analyses were performed to investigate the potential interaction between polymers and drugs for the preparation of samples (**Figure 3**). The main absorption peaks of pure PVA were observed at 3268 cm^{-1} (O—H stretching vibration of the hydroxy group), 2915 cm^{-1} (C—H asymmetric stretching vibration), 1649 cm^{-1} (C═O carbonyl stretch), 1414 cm^{-1} (C—H bending vibration of CH_2), 1084 cm^{-1} (C—O stretching of acetyl groups), and 834 cm^{-1} (C—C stretching vibration).[37,38] PEG showed O—H stretching vibration, alkyl (—CH_2) stretching, —CH_2 binding vibration, and ether (C-O-C) stretching group at 3272, 2879, 1466, and 1097 cm^{-1}, respectively.[39,40] PLGA exhibited the major characteristic peaks at 3360, 2920, 2800, 1268, and 1047 cm^{-1} due to the presence of O—H, C—H, CH_3, C—O, and C═O functional groups. The characteristic infrared bands of DO were seen as sharp peaks due to the O—H, C═O stretch, C—N—C stretch, and C—H swing bands at 3585, 1681, 1477, and 1313 cm^{-1}, respectively.[41–43] According to these results, it was approved that the produced samples consisted of the DO and other polymers.

2.3. X-Ray Powder Diffraction (XRD)

The crystalline natures of polymers, drugs, and drug carrier systems are shown in **Figure 4**. PLGA exhibited broadened and reduced intensity and number of peaks because of having a dominantly amorphous structure. A broad peak belonging to PLGA was seen between 10° and 27°. The unbalanced PLGA pattern was obtained after 30° due to the hydrolysis of small PLGA pieces or an unbalanced PLGA particle size distribution.[29,44] Sharp

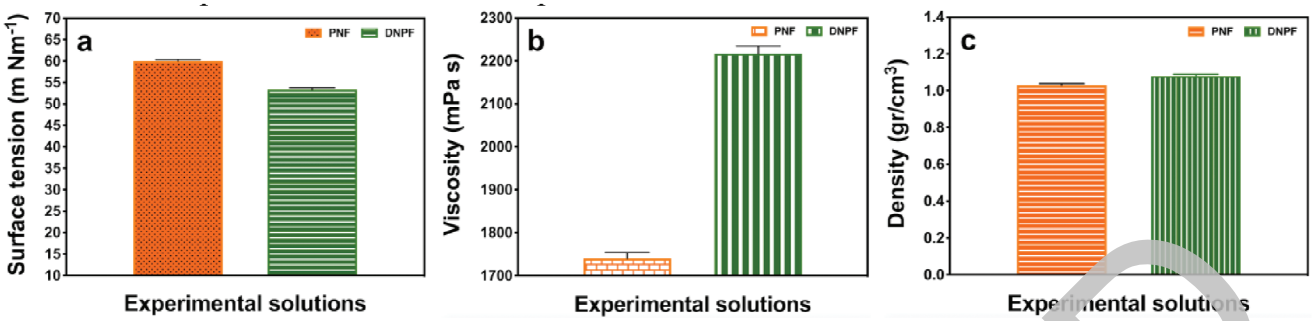

Figure 1. Physical parameters of the PVA/PEG solution: a) Surface tension, b) viscosity, and c) density.

peaks were observed in the DO pattern due to its crystalline structure. Furthermore, similar peaks in the DO pattern were determined in DNP diffractograms. However, the appearance of characteristic DO sharp peaks reduced after the incorporation of DO into PLGA NP due to the effect of the PLGA amorph structure.[29,44,45] In the PVA structure, two peaks with a semicrystalline character were clearly visible at $2\theta = 20.1°$ and 40.8°. This semicrystalline nature originated from a strong intramolecular and intermolecular hydrogen bonding between PVA and OH groups. The presence of PEG provided to be seen a peak at $2\theta = 10.5°$. PEG caused the semicrystalline nature of PVA to be reduced by hydrogen bonding formation.[46–48]

2.4. Differential Scanning Calorimetry

Differential scanning calorimetry (DSC) thermograms were analyzed to investigate the thermal properties of samples. An endothermic peak related to the glass transition temperatures (T_g) of PLGA was observed at 68.1 °C for PNP. It was no melting point because of the amorphous nature of PLGA. A sharp melting endotherm peak (Tm) was obtained in the presence of the crystalline structure of DO at 224.4 °C. After loading of DO to PLGA nanoparticles, its melting point was seen at the same temperature, however, its sharpness decreased. The increased free volume between the chains of the polymer due to the effect of plasticizers causes it to rotate and move the chain segments more freely. This situation leads to a decrease in the T_g and Tm values of the polymer. DNP showed its T_g value at 63.5 °C because of the interaction of the drug and PLGA. DO acted like a plasticizer due to its crystalline structure and led the T_g value to decrease. These results showed that DO was in a dissolved and dispersed state in DO-loaded PLGA nanoparticles.[29,49–51] During the PVA and PEG blending process, a decrease in the PVA crystallinity is observed because of the between PVA and PEG H-bonding formation causing the PVA chain mobility reduction. DNPF showed a sharper Tm peak at 225.2 °C due to the crystalline structure of DO [52] (**Figure 5**).

2.5. In Vitro Drug Release Profiles Evaluation

In this study, the main aim is to improve a brain-targeting novel drug-delivery system, which reduces the dosage frequency and side effects and increases the bioavailability of drugs for the treatment of AD. Therefore, biocompatible, biodegradable, hydrophobic PLGA polymer was chosen to provide sustained drug release for loading DO. The EE of DNP and DNPF were detected by 88.7 ± 1.1 and 86.7 ± 1.3%. Then, an in vitro drug release test was performed to investigate the encapsulated DO release profile from DNP in PBS by mimicking the plasma pH (pH 7.4, at 37 °C) for 18 days. DNP exhibited a biphasic release pattern with an initial burst release followed by sustained release. It was observed the initial burst drug release within the first 6 h due to the entrapped DO molecules in the surface layer of the PLGA NPs, which directly dissolve when the nanoparticles are put in the PBS. The other reason can be the small size of particles causing faster diffusion. After releasing almost 50% of the drug amount from DNP in the first 6 h, the drug release profile reflected the entrapped DO in the PLGA matrix by decreasing the release rate. 57.3%, 67.1%, 87.7%, and 99.6% of DO were released from the DNP at the end of the 1st, 3rd, 10th, and 18th days.[29,53] The 5 different release kinetic models, which are the first order, Hixson-Crowell, Krosmeyer-Peppas, Higuchi, and zero order, were used to analyze the release kinetic of DO from DNP. DO was released according to the first order kinetic model with higher R^2 values (0.9586.) The first order model refers to a system, whose drug release rate is only a function of the remaining drug concentration. Also, it depends on the surface changes over time.[54–56] The diffusion exponent value (n) was calculated to depict the release mechanism. This value was found to be less than 0.45. Based on this result, DO was released from DNP by a quasi-Fickian diffusion mechanism [57] (**Table 2**). Furthermore, the strong interchain interactions via the hydrogen bonding formation and the regularity of the chain may affect the quasi-Fickian diffusion mechanism.[58] It indicates that DO diffuses from partially water-filled pores in the DNP through a swollen matrix with little erosion involvement [59] (**Figure 6**). In this study, DNPF was used to facilitate the dosage adjustment and sublingual administration of DNP. For this reason, the disintegration test of DNPF produced using PVA and PEG, which are water-soluble polymers, was performed and it was proved that it was completely disintegrated in 2 s, thus the prolonged controlled released DNPs embedded in it passed into the systemic circulation in the salivary fluid at the end of 2 s (**Figure 7**).

2.6. Disintegration and Wetting Test

The rapid disintegration and short stay in the mouth are one of the most crucial parameters for drug absorption to mucosa blood vessels after sublingual administration. The drug carrier system should be disintegrated in saliva rapidly. Therefore, the drug can

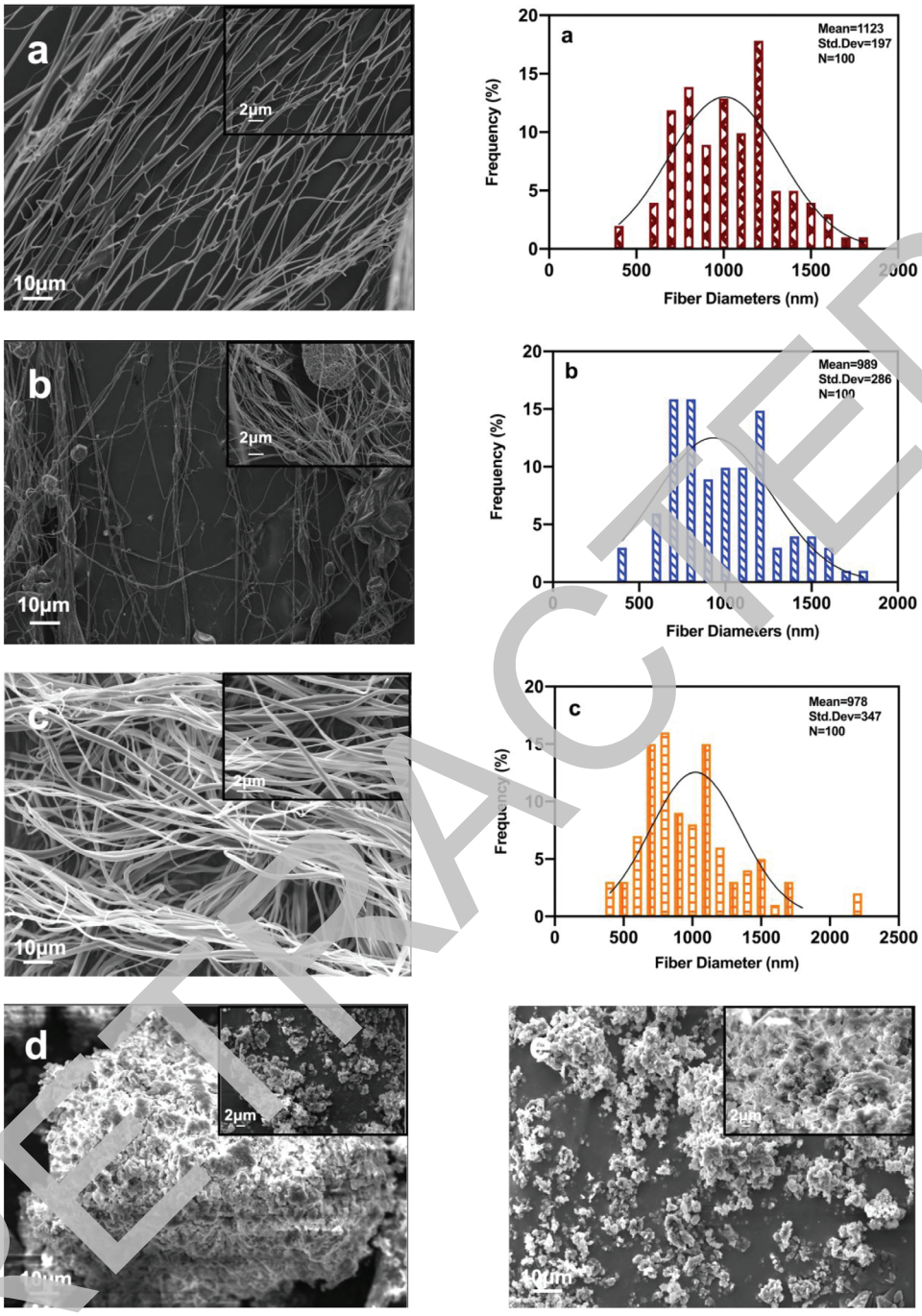

Figure 2. SEM images and diameter distribution graphs of the pure PVA/PEG fibers (PNF) at three different ratios: a) 8:1, b) 9:1, and c) 10:1 (v/v), d) pure PLGA nanoparticle (PNP), e) donepezil (DO)-loaded PLGA nanoparticles (DNP), f) DNP-loaded PVA/PEG fibers (DNPF) (10:1, v/v), and g) fluorescence microscopy of DO-loaded PLGA nanoparticles (DNP). N = 100 in all diameter distributions.

be protected from the hepatic first-pass effect and gastric degradation, in contrast, providing a faster absorption [60,61] The material properties, which are used to produce nanofibers, affect the disintegration time.[62] Hence, PVA and PEG, which are water-soluble polymers, were chosen to produce nanofibers. 2 min is accepted as the valid time limit for the disintegration test according to the USP for the sublingual route.[63] These results showed that this new drug carrier system has ultra-fast disintegrated properties via disintegration within 2 sec for the sublingual route. Therefore, it was clearly seen that the DNP in these nanofibers can be rapidly absorbed without any chance of it being swallowed. Normally, 100% bioavailability can be achieved by administering nanoparticles by intravenous (IV) administration, but this route of drug administration can be performed under the control of a

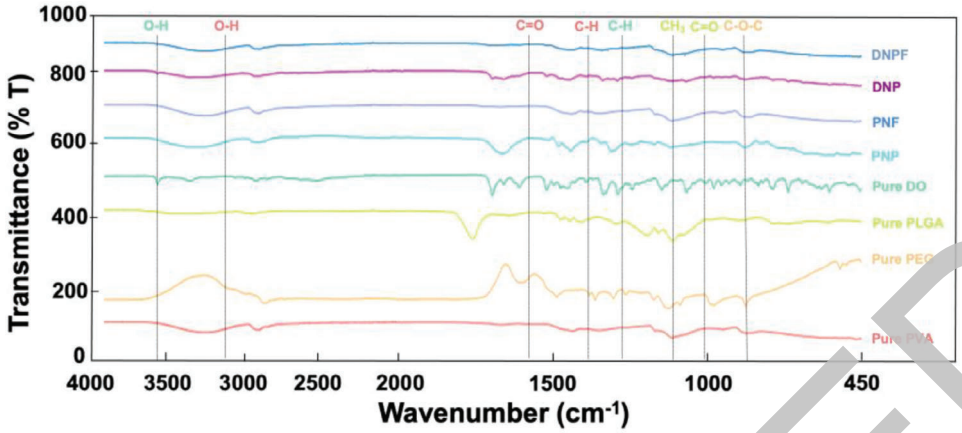

Figure 3. The FT-IR spectrum of pure PVA, PEG, PLGA, donepezil (DO), pure PLGA nanoparticles (PNP), pure PVA/PEG nanofibers (PNF), DO-loaded PLGA nanoparticles (DNP), and DNP-loaded PVA/PEG nanofibers (DNPF).

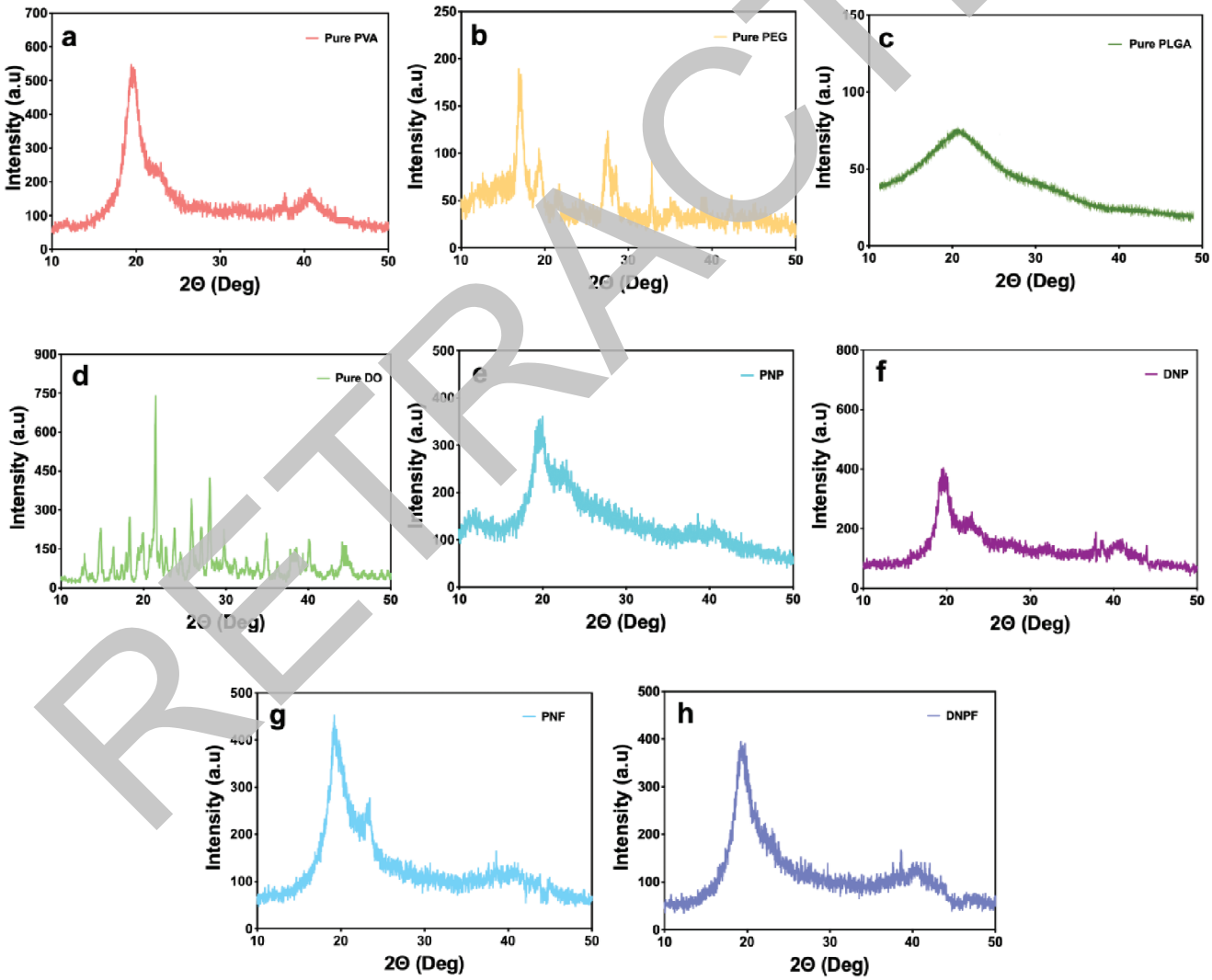

Figure 4. Results of XRD analysis: a) Pure PVA, b) pure PEG, c) pure PLGA, d) pure donepezil (DO), e) pure PLGA nanoparticles (PNP), f) DO-loaded PLGA nanoparticles (DNP), g) pure PVA/PEG nanofibers (PNF), and h) DNP-loaded PVA/PEG nanofibers (DNPF).

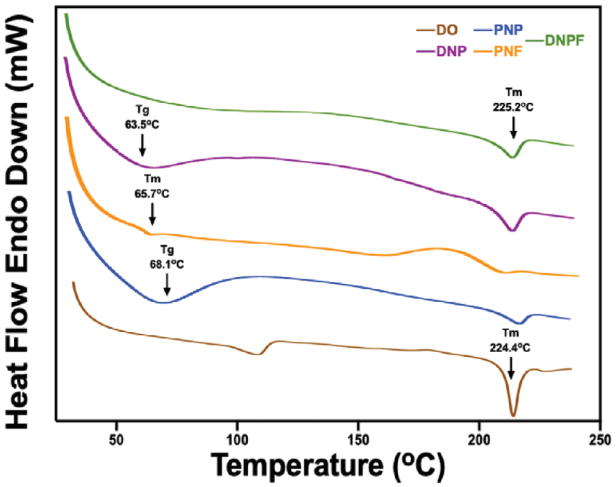

Figure 5. DSC results of pure donepezil (DO), pure PLGA nanoparticles (PNP), DO-loaded PLGA nanoparticles (DNP), pure PVA/PEG nanofibers (PNF), and DNP-loaded PVA/PEG nanofibers (DNPF).

Table 2. Diffusional release mechanism interpretation according to the ranges of n value.

n value	Diffusion Mechanisms
n<0.45	Quasi-Fickian Diffusion
0.45	Fickian Diffusion
0.45<n<0.89	Anomalus (Non-Fickian) Diffusion
0.89-1	Case II Transport (Zero Order Release
n>1.0	Super Case II Transport

physician and can cause pain. However, in this study, by loading nanoparticles into a drug carrier system suitable for sublingual administration, nanoparticles were transformed into an easy-to-use, painless, and highly bioavailable form (Figure 7).

2.7. In Vitro Cell Culture

2.7.1. Cell Viability Assay

The cytocompatibility of PNF, PNP, DNP, and DNPF was evaluated to investigate their effects on cell proliferation in SH-SY5Y cells by utilizing the alamarBlue reagent after a 24 h incubation. Drug-loaded samples were applied in 3 different dosages at 1, 5, and 10 μM.[31] Raw DO was utilized as a positive control group. The test showed that all samples exhibited above ≈90% cell viability via their nontoxic natures. The cell proliferation improved expressively as increasing the amount of drug-exposed. However, no significant difference was realized between raw DO at 5 and 10 μM. PLGA, PVA, and PEG polymers are approved as safe by FDA.[64,65] Also, in this study, PNP and PNF exhibited noncytotoxic behaviors due to selected polymers. According to these results, produced nanoparticles and nanofibers might be promising delivery systems (**Figure** 8a).

2.7.2. Neuroprotective Effect Evaluation

The neurotoxic and neuroprotective efficacy has been evaluated in Aβ_{1-42}-induced SH-SY5Y cell cytotoxicity accepted as an in vitro AD model. The SH-SY5Y human neuroblastoma cell line is frequently preferred for mimicking neurodegenerative disease studies such as Parkinson's disease and AD, as an in vitro model. SH-SY5Y cells are derived from an immature neuronal lineage in the sympathetic nervous system. These cells can express immature neuronal proteins, continuously proliferate, and acquire mature neuron-like features. After neuronal differentiation, SH-SY5Y neuroblastoma cells perform various morphological and biochemical events, namely the formation and extension of neurites, a decrease in proliferation rate, and mature neuronal markers expression. Besides, the most important thing is that SH-SY5Y cells express human proteins.[66–68] To create the fibril or oligomers, the Aβ_{1-42} peptide (at 20 μM) was incubated for 24 h in media containing SH-SY5Y cells in this study.[69] The cells were treated with DO, DNP, and DNPF at 1, 5, and 10 μM, and compared the cell viability ratio with the untreated Aβ_{1-42}-induced and control groups. Higher cell viability was observed compared to the untreated Aβ_{1-42}-induced group. Also, the anti-Alzheimer effects of DNP and DNPF at 1 μM were found better than the other treatment groups at 5 and 10 μM. However, no significant difference was obtained between the different concentrations of treatment groups. DO derivatives were applied in the same dosages as a kind of treatment on the Aβ_{1-42}-induced SH-SY5Y cell line in the literature and all DO derivatives were found to have neuroprotective effects including 1 μM in that study.[70] On the other hand, the untreated Aβ_{1-42}-induced group caused cell viability to decrease to 35.7%. Krishna et. al obtained a similar decrease after inducing Aβ_{1-42} compared to the control group.[71] All treatment groups are found effective for the treatment of AD (Figure 8b).

2.7.3. Cell Uptake and Anti-Alzheimer's Activity

The study investigates the comparative effects of DNPF and a DO suspension in PBS (DNP-PBS) on HNPCs, and ADCs, which were developed by transfecting HNPCs with an AP-APP plasmid. As shown in **Figure** 9A, the relative intensity analysis before and after transfection indicates that post-transfection ADCs exhibit significantly elevated levels of tau and Aβ proteins compared to pre-transfection HNPCs, confirming the successful generation of the AD model. Figure 9C illustrates the enhanced cellular uptake of DNPF, which is more pronounced than that of DNP-PBS or control treatments, as demonstrated by the dye conjugation study.

Furthermore, as highlighted in Figure 9D, DNPF leads to a significantly higher relative intensity of tau and Aβ protein expression compared to DNP-PBS, with both formulations showing increased levels compared to controls. This effect is also confirmed by the Western blot results in Figure 9B. The enhanced cellular uptake and increased protein expression observed with DNPF may be attributed to the improved delivery mechanism of the nanoparticles. Additionally, DO is known to inhibit AChE, thereby increasing acetylcholine levels in the brain and alleviating symptoms of AD.[72,73] The integration of DO into PLGA

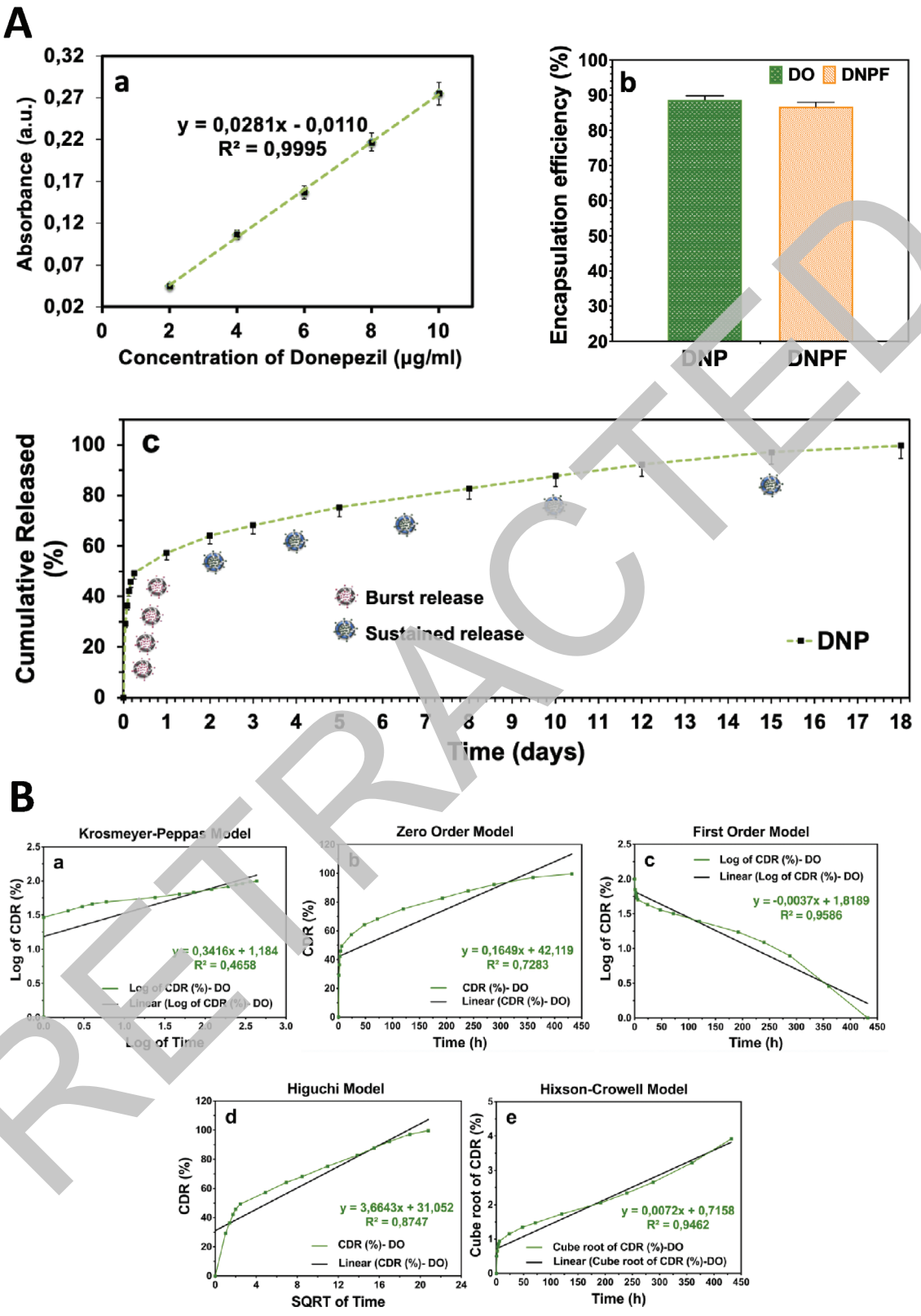

Figure 6. A) In vitro drug release profile of donepezil (DO)-loaded PLGA particles (DNP): a) calibration curve of DO, b) DNP encapsulation efficiency, and c) release profiles DO for 432 h. Three repeats of each measurement were done, and the errors were all under 5%. B) The release kinetic models of DO from DNP: a) Korsmeyer-Peppas, b) zero order, c) first order, d) Higuchi, and e) Hixson-Crowell models.

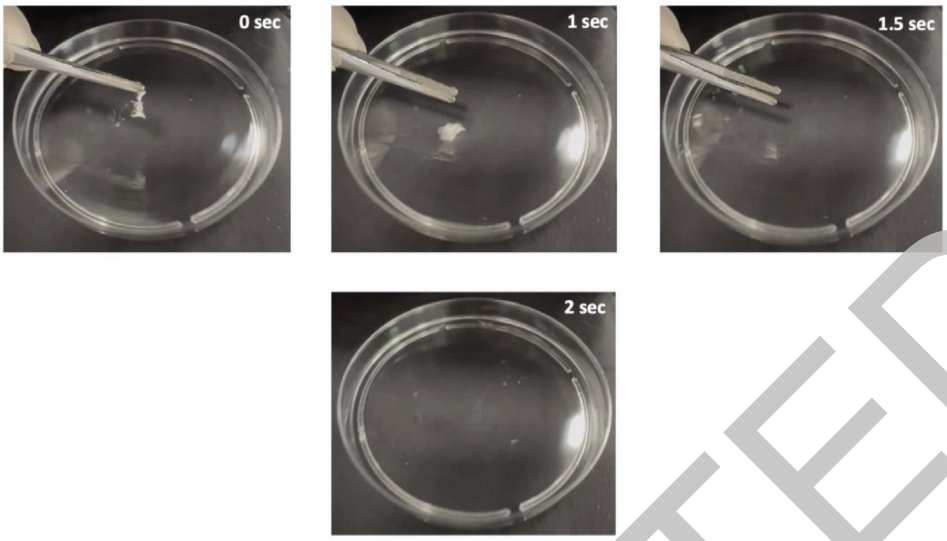

Figure 7. Images of donepezil (DO)-loaded PLGA particles (DNP)-loaded PVA/PEG nanofibers (DNPF) at several time points during the disintegration test.

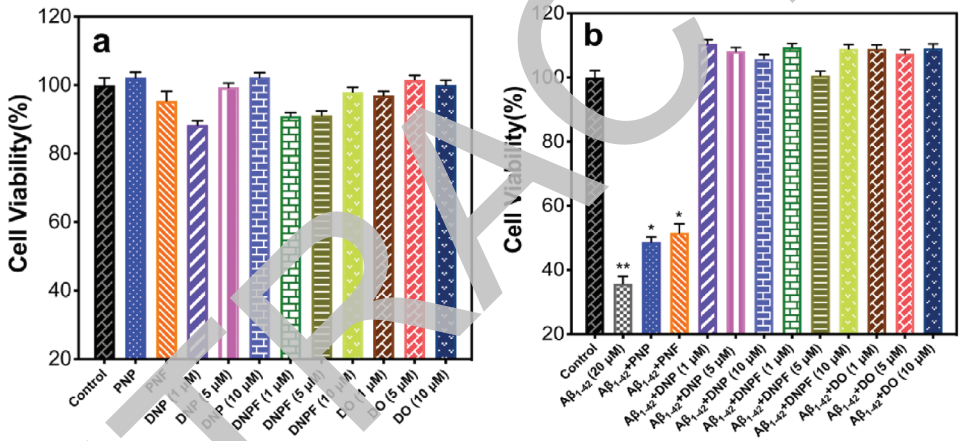

Figure 8. In vitro cellular evaluation in SH-SY5Y cells: a) Cell viability and b) neuroprotective effect evaluation of treatments. Significance differences were found at *$p < 0.05$ and **$p < 0.01$ compared to the control group.

nanoparticles may further enhance its therapeutic efficacy by providing a sustained release and targeted delivery, potentially reducing cholinergic side effects and improving cognitive outcomes. This study's findings suggest that DNPF, as a novel delivery system, may offer superior therapeutic benefits over conventional DO formulations, particularly in the context of AD therapy.[74,75]

3. Conclusion

In this study, PNF was produced by PG at three different ratios, which are 8:1, 9:1, and 10:1 (v/v). The ratio of 9:1 was chosen as the optimized ratio and DNP was embedded in this ratio. According to the SEM images, the diameters of nanofibers increased after loading DNP. FT-IR results showed that produced nanoparticles and fibers consisted of the DO and other polymers. The sharp peaks of DO in the XRD patterns were reduced after the incorporation of DO into PLGA NP due to the effect of the PLGA amorph structure. The semi-crystalline nature of PVA was reduced because of PEG by hydrogen bonding formation. The T_g value of DNP decreased after loading DO because of the interaction of the drug and PLGA. On the other hand, the Tm value of powder DO did not change after loading DO to nanoparticles and nanofibers, however, the sharpness of DSC curves of DNP and DNPF decreased compared to powder DO. The in vitro drug release test of DNP was performed for 18 days. It was obtained that presented that 57.3%, 67.1%, 87.7%, and 99.6% of DO were released from the DNP according to the Hixson-Crowell Release kinetic model at the end of 24 h, 3rd, 10th, and 18th days, respectively. DNPF totally disintegrated within 2 s and demonstrated ultra-fast disintegration properties for the sublingual route. According to the alamarBlue test results, there was no cytotoxicity effect. DNP and DNPF at 1 μM presented a better anti-Alzheimer's effect than the other treatment groups on the $A\beta_{1-42}$-induced SH-SY5Y cells. These findings, supported

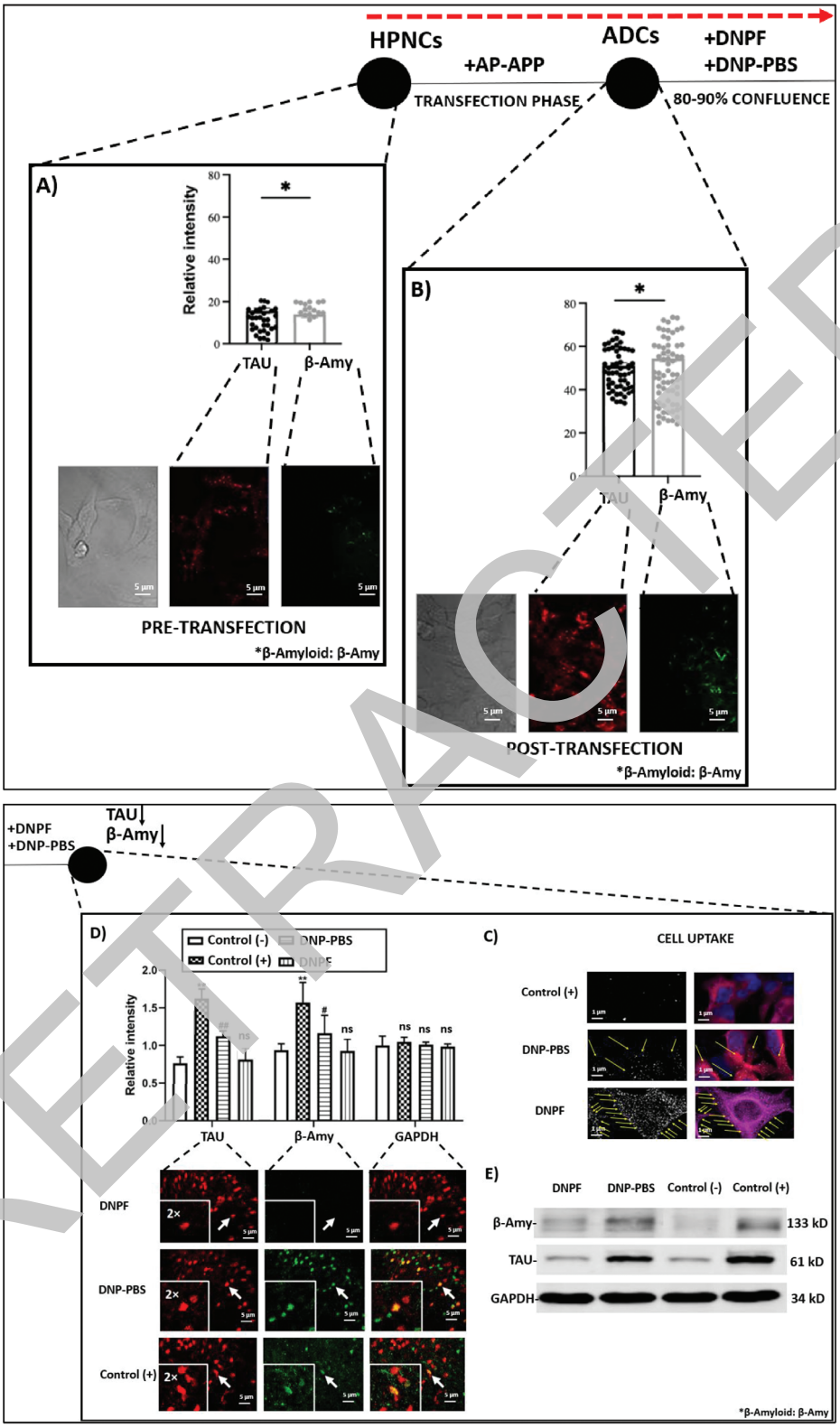

Figure 9. Comparative analysis of donepezil (DO)-loaded PLGA particles (DNP)-PBS and DNP-loaded PVA/PEG nanofibers (DNPF) on Alzheimer's disease (AD) Markers in human neural progenitor cells (HNPCs) and AD cells (ADCs): A) Pre- and Post-Transfection Analysis of tau and Aβ expression in HNPCs, B) Evaluation of cellular uptake in ADCs treated with DNPF compared to DNP-PBS, and controls, C) Relative intensity of tau, amyloid beta (Aβ), and GAPDH in different treatment groups, D) Western blot analysis of protein expression post-treatment. *Control (-): Untreated and Alzheimer negative group-HNPCs, Control (+): Untreated and Alzheimer positive group.

by enhanced cellular uptake and significant modulation of tau and Aβ protein expression as shown in the study, suggest that DNPF could be a highly effective new strategy for AD treatment.

4. Experimental Section

Chemicals: Donepezil (DO, Mw ≈ 379 492 g mol^{-1}) was kindly provided by Sanovel Pharmaceutical (Istan- bul, Turkey). Polyvinyl alcohol (PVA, Mw ≈ 89 000–98 000), polylactic-co-glycolic acid (PLGA, Mw ≈ 24 000—38 000), polyethylene glycol (PEG, Mw ≈ 4000), diazo dye (Congo red) (#C6767), pFTAA live-cell dye (#SCT066), X-tremeGENE siRNA Transfection Reagent (#SITRAN-RO), and amyloid $\beta_{1\text{-}42}$ (A$\beta_{1\text{-}42}$) were purchased from Sigma–Aldrich (St. Louis, MO, USA). Human neural progenitor cells (HPNCs) (#ACS-5005) were sourced from ATCC (Waltham, MA, USA). AP-APP plasmid (#196 706) was a gift from Martino Calamai (Addgene, RRID: Addgene_196 706). Human β-Amyloid 1–42 Antibody (#01 567), mAb, Mouse and Tau Antibody (Phospho-Thr217), pAb, Rabbit (#A00896), were acquired from Genscript (Piscataway, NJ, USA). RPMI 1640 medium and fetal bovine serum were provided from Servicebio (Wuhan, China). All purchased materials are of analytical grade.

Methods: *Preparation and Characterization of PLGA Nanoparticles*: Utilizing a dual emulsion (water/oil/water) solvent evaporation process, a pure PLGA nanoparticle (PNP) was created. Dichloromethane was used to dissolve 40 mg of PLGA in 2 mL. 200 µL of PEG was utilized to dissolve 50 µg of DO, which was then homogenized. To create a water/oil/water emulsion, the mixture was then added to 50 mL of PVA solution (1 wt.%) and homogenized. A magnetic stirrer was employed to remove extra dichloromethane from the mixture solution. The produced nanoparticles were centrifuged at 12 000 rpm for 20 min to separate them. After that, it was lyophilized for drying and rinsed three times with deionized water to produce higher-purity nanoparticles. The physical characterization experiments were performed using a Zetasizer Nano ZS 90 (Malvern Instrument, UK). Each nanoparticle was measured three times, and a deionized water solution was employed at a temperature of 25 °C.[76]

Preparation and Characterization of Nanofibers: PVA (17%, w/v) and PEG (80%, w/v) were dissolved in distilled water at 120 °C and room temperature, respectively. PVA/PEG was mixed 8:1, 9:1, and 10:1 (v/v) ratios, respectively. All produced pure nanofibers (PNF) morphologies were analyzed by using SEM, and the best one as having uniform and beadless morphology was chosen at 10:1 (PVA/PEG) ratio. Therefore, DNP was added as 0.9–1.4 mg mL^{-1} into the PVA/PEG (10:1) composite solution. The best production of DNPF by PG was obtained at 1.1 mg mL^{-1} of DNP.

A density bottle (10 mL density bottle, Boru Cam Inc., Turkey), a DV-E viscometer (Brook eld AMETEK, USA), and a force tensiometer (Kruss K9, Hamburg, Germany) were employed to measure the physical properties of all polymer solutions. Each measurement was performed three times at a temperature of 25 °C. Measurements began with a calibration of the equipment.

All PNF and DNPF were created by PG utilizing a technique that was previously discussed.[77] In summary, 1 mL of solutions was put into an aluminum vessel and spun at a rotational speed of between 9000–15 000 rpm, a working pressure of between 1.5–3.5 MPa, a humidity of between 35%–40%, and a temperature of between 30–37 °C to produce fibers. The best production of nanofibers was found at 12 000 rpm, 3 atm, 36.7% humidity, and 36.4 °C.

Scanning Electron Microscopy: The fibers' diameter and morphology were examined using a scanning electron microscopy (SEM) (EVO LS 10, ZEISS equipment). Prior to SEM, all samples' surface was coated with gold for a min. By measuring the diameter of 100 fibers in a sample of micrographs chosen at random and using ImageJ software (Broken Symmetry Software), the mean diameter and fiber size distribution were determined.

Fourier Transform Infrared Spectroscopy: Fourier transform infrared spectroscopy (FT-IR) measurements were realized using a Jasco FT/IR 4700 spectrometer and spectrographs were analyzed using OPUS Viewer version 6.5 software to determine the molecular contents of fibers and particles to confirm the presence of PLGA, PVA, PEG, and DO. Measurements were obtained between 500 and 4000 cm^{-1} wavenumbers with a resolution of 4 cm^{-1} at room temperature.

X-ray Powder Diffraction (XRD): Using a D/Max-BR diffractometer (RigaKu, Tokyo, Japan) with Cu Kα radiation, the structure and crystalline morphologies of the nanofibers and nanoparticles were examined. At a rate of 2°/min, analyses were conducted at 40 mV and 30 mA throughout a 2 range of 5–50°. The acquired data were converted to diffractograms using OriginPro 7.0 software (OriginLab Corporation, MA, USA), and the results were used.

Differential Scanning Calorimetry (DSC): Differential scanning calorimetry (DSC) analysis was carried out using Pyris software and Perkin Elmer Jade DSC (PerkinElmer Inc., Massachusetts, USA). To examine the thermal characteristics of fibers and particles, the system was set up with a heating rate of 10 °C min^{-1} between 0 and 200 °C and a dynamic argon atmosphere (20 mL min^{-1}). Measurements began with a calibration of the equipment.

Evaluation of Encapsulation Efficiency of DNP and DNPF: The quantity of drug that had been incorporated into nanofiber and nanoparticles relative to the initial amount of drug utilized to create the formulation was known as encapsulation efficiency (EE). In order to determine the DO content in nanofibers and nanoparticles, the standard assay technique was used. First, the standard calibration curve of DO was created by measuring the absorbance of the DO at various concentrations at a wavelength of 272 nm, and a spectral line equation was acquired. The line equation was used to determine how much DO was present in the supernatant. For the EE, the nanofiber and nanoparticles entirely dissolved in the appropriate solvents. In a volumetric flask, they were weighed (5 mg) and dissolved in 3 mL of their respective solvent mixes. To ensure the entire dissolution of DO from nanoparticles into the solvent, the flask was gently swirled for 1 h. Using a UV–vis spectrophotometer (Jenway 6305, Bibby Scientific, Staffordshire, UK) at 272 nm, 1 mL of the solution was taken and tested. Equation (1) was used to calculate the % EE. Each measurement was made in triplicate.[3,77]

$$\text{EE} = \text{mass of actual drug loaded in fibrous scaffolds} / \text{mass of drug used in fibrous scaffolds fabrication} \quad (1)$$

In Vitro Drug Release Assay: *In vitro* drug release assay was done to investigate the release kinetics of DO from nanoparticles. DNP was weighed 60 mg in order to evaluate the drug release profiles. Samples were immersed in 1 mL of PBS (pH 7.4 at 37 °C) for a period of 18 days. At the end time intervals (1st, 2nd, 3rd, 4th, 6th, 24th, 48th, 72nd, 120th, 192nd, 240th, 288th, 360th, and 432nd h) to continue the release test, 1 mL of PBS was withdrawn from each sample container and fresh PBS in the same volume was added. The amount of released DO at 272 nm was measured using UV spectroscopy (Jenway 7315, Bibby Scientific, Staffordshire, UK). A linear calibration curve of standard solutions was created at the start of drug release studies. DO was prepared in 5 different concentrations (2, 4, 6, 8, and 10 µg mL^{-1}) to construct a linear calibration curve Analysis of DO drug release behaviors was done. The experiments were carried out three times.[76]

In Vitro Release Kinetic Test: The release of the DO from the DNP was calculated using different mathematical models for the in vitro simulation of the DO changes in the plasma concentration of the body over time. The equations below have variables that belong to Krosmeyer-Peppas (Equation (2)), zero order (Equation (3)), first order (Equation (4)), Higuchi (Equation (6)), and Hixson-Crowell (Equation (6)) models.[78] The kinetic constants of these models are K, K_0, K_1, K_h, and K_{hc}, respectively. Q represents the drug release's fractional amount at time t. The diffusion exponent is indicated by n.

$$Q = Kt^n \quad (2)$$

$$Q = K_0 t \quad (3)$$

$$In\,(1 - Q) = -K_1 t \quad (4)$$

$$Q = K_h t^{1/2} \quad (5)$$

$$Q^{1/3} = K_{hc} t \quad (6)$$

Disintegration and Wetting Test: Using a biopsy cutter, a circular segment of the fibers measuring 30 mm in diameter was taken, and it was then put in a petri dish with 15 mL of simulated saliva (pH 6.8). Potassium chloride 0.062%, methyl-paraben 0.2%, potassium phosphate 0.034%, magnesium chloride 0.005%, dextrose 4.69%, sodium carboxymethylcellulose 0.5%, and sodium fluoride 0.01% (wt. percent) were the ingredients in the formulation of the artificial saliva used in the current analysis.[79] Warm water (30—35 °C) was used to dissolve methylparaben, dextrose, and magnesium chloride. Before blending the solutions at room temperature, this solution was cooled down.

A video camera (Canon Sx70 HS, Tokyo, Japan) was used to record the fibers' wetting and disintegration at 50 frames per sec.

In Vitro Cell Culture Tests: *Preparation of Oligomeric $A\beta_{1\text{-}42}$ and Treatment Stock Solutions*: $A\beta_{1\text{-}42}$ stock solution was prepared using PBS at a concentration of 1 mg mL^{-1} and a pH of 7.4 at 37 °C. The stock solution was incubated at 37 °C for 72 h. The stock solutions of the treatments, which are DNP, DNPF, and raw DO, were prepared with PBS at the concentrations of 1, 5, and 10 µM before 24 h. Therefore, DO was released from nanoparticles and nanofibers for a day.

Cell Culture and Treatments: The differentiated SH-SY5Y cells were cultured in 90% RPMI 1640 medium (Servicebio, Wuhan, China) with 10% fetal bovine serum at 37 °C in an incubator with a humidified environment and 5% CO_2. Cells were passaged by trypsinization every 3 days. For the assay, SH-SY5Y cells were sub-cultured for 24 h in 96-well plates at a seeding density of 0.5×10^4 cells $well^{-1}$. The cells were incubated for another 24 h in the presence of $A\beta_{1\text{-}42}$ at the concentration of 20 µM to induce AD. After $A\beta_{1\text{-}42}$ induction, cells in the treatment groups were exposed to stock solutions of DO for 24 h at varied concentrations of 1, 5, and 10 µM. One group of cells was maintained without drugs or $A\beta_{1\text{-}42}$ as the vehicle control. After the treatment, the morphological structures of cells in each group were observed by the phase contrast microscope.[69,70]

AlamarBlue Assay for Assessment of Cell Viability: AlamarBlue fluorescent measurements were acquired after a day to evaluate cell vitality and attachment. The alamarBlue assay is based on a redox indicator that transforms from an oxidized (blue) substrate taken up by the cells to a reduced (red) form as a result of dehydrogenase activity within the metabolically active cells. After 24 h from the seeding of cells to 96-well plates, the samples of nanoparticle and nanofiber were applied to cells. After another 24 h, 10 µL of the alamarBlue working solution was added to each group followed by 4 h of incubation at 37 °C. A fluorescence plate reader (PR4100 Absorbance Microplate Reader, Bio-Rad, UK) was employed to detect absorbance at 570 nm.[80]

Protection of SH-SY5Y Cells Against $A\beta_{1-42}$-Induced Damage: SH-SY5Y cells were seeded in 96-well plates at 0.5×10^4 per well and cultured at 37 °C for 24 h. $A\beta_{1-42}$ (20 µM) were added into cells. The plates were again incubated for an additional 24 h at 37 °C. Then, the treatment groups of DO at 1, 5, and 10 µM were applied to the cells. After 24 h, using the alamarBlue assay methodology, cell viability was measured and presented as a percentage of the control cells.[70]

AP-APP-linked Vector Related ADC Model, Endocytosis, and Inhibition Mechanism of DNPF: To assess the endocytosis efficiency of DNPF in progenitor neural cells, the HNPCs were cultured in appropriate conditions until they reached 50%–60% confluency (*This confluency is preferred as it is necessary for transfection*). The AP-APP plasmid was introduced into the HNPCs using a transfection reagent (SITRAN-RO). The transfection mixture was prepared by combining 1.5 µL of SITRAN-RO with 0.3 µg of siRNA. This mixture was then applied to HNPCs that are at 50% confluence, with the transfection carried out in the presence of 10% fetal bovine serum (FBS). Post-transfection, the cells were incubated for 24–48 h to allow sufficient expression of the plasmid.[81] DNPF was treated in the culture medium at a predetermined concentration (1 µM). After a 24 h incubation period, the AD cells (ADCs) were washed with PBS to remove any non-internalized DNPF. The efficiency of endocytosis was evaluated by analyzing the intracellular uptake of DNPF using flow cytometry (BD FACSymphony, BD Biosciences, Franklin Lakes, NJ, USA).

For the fluorescence microscopy analysis of tau and Aβ, specific fluorescent dyes were applied to the cells according to the manufacturer's instructions. The cells were then fixed with paraformaldehyde and mounted on slides. Leica DM750 P Polarizing (Hesse, Germany) was used to capture images of the stained tau and Aβ aggregates.

Western Blot and RT-PCR with ADCs: After 24 h incubation period, ADCs were homogenized in a high-salt reassembly (RAB) buffer to isolate the RAB-insoluble fractions. After centrifugation, the resulting pellets were further homogenized in RIPA buffer and subjected to another round of centrifugation. The RIPA-insoluble pellets were then extracted with 75% formic acid (FA) to obtain the FA fractions. Centrifugation was performed at 4000 rpm for 30 min. Protein concentrations from each fraction were normalized, and equivalent amounts of protein were separated on a 10% NUPAGE gel before being transferred to a blot. To ensure equal loading and rule out contamination of the FA fraction with soluble proteins, the blots were probed with a GAPDH-specific monoclonal antibody. For quantification, the blots were also probed with antibodies specific to tau and $A\beta_{1\text{-}40}$, and the images were analyzed using Image Lab Touch Software (BIO-RAD, Hercules, CA, USA).

Real-Time Quantitative PCR: Real-time quantitative PCR was conducted for Aβ, tau, and GAPDH using specific primers, with GAPDH serving as a housekeeping control. Cycle threshold (ΔΔCt) values were calculated using TSA Software (v1.4.0.1, Applied Bioscience, Waltham, MA, USA). The inhibition efficiency of DNPF was determined by comparing the levels of these proteins in treated versus untreated cells.

Statistical Analysis: The statistical application GraphPad Prism 8.0 was used to analyze the data statistically. Except for the fiber distribution graphs, which were provided as mean standard deviation, results were presented as the mean standard error of the mean. ANOVA and the Tukey post hoc test were utilized to evaluate the performance of the groups between them. Values with $p < 0.05$ were considered significant.

Acknowledgements

The authors dedicate this article to the memory of Turkish citizens, who lost their lives in the earthquakes held in Pazarcık and Elbistan – Kahramanmaraş and Hatay, Türkiye on February 06, 2023.

Conflict of Interest

The authors declare no conflict of interest.

Author Contributions

E.G., H.B.Y., and B.U. performed investigation, methodology, visualization, wrote the original draft, wrote, reviewed and edited. M.D. performed production of nanoparticle, wrote the original draft. A.A. performed cell culture investigation, and wrote the original draft. F.I., Y.Y., O.G., and D.M.K. performed investigation and methodology, and wrote the original draft. M.E.C. performed conceptualization, validation, wrote the original draft, supervision, wrote, reviewed and edited, and funding acquisition.

Data Availability Statement

The data that support the findings of this study are available from the corresponding author upon reasonable request.

Keywords

Alzheimer's disease, Alzheimer's disease cell model, AP-APP plasmid transfection, donepezil, drug delivery, nanofiber, nanoparticle

Received: April 30, 2024
Revised: September 4, 2024
Published online: October 24, 2024

[1] D. S. Knopman, H. Amieva, R. C. Petersen, G. Chételat, D. M. Holtzman, B. T. Hyman, R. A. Nixon, D. T. Jones, *Nat. Rev. Dis. Primers* **2021**, *7*, 33.
[2] L.-K. Huang, S.-P. Chao, C.-J. Hu, *J. Biomed. Sci.* **2020**, *27*, 1.
[3] F. Topal, B. Ertas, E. Guler, F. Gurbuz, G. S. Ozcan, O. Aydemir, V. G. Bocekci, G. Duruksu, C. S. Cam, Y. Yazir, *Biomater. Adv.* **2022**, *138*, 212870.
[4] R. Ismail, P. Parbo, L. S. Madsen, A. K. Hansen, K. V. Hansen, J. L. Schaldemose, P. L. Kjeldsen, M. G. Stokholm, H. Gottrup, S. F. Eskildsen, *J. Neuroinflammation* **2020**, *17*, 151.
[5] M. B. Colovic, D. Z. Krstic, T. D. Lazarevic-Pasti, A. M. Bondzic, V. M. Vasic, *Curr. Neuropharmacol.* **2013**, *11*, 315.
[6] N. Kumar, A. Gahlawat, R. N. Kumar, Y. P. Singh, G. Modi, P. Garg, *J. Biomol. Struct. Dyn.* **2022**, *40*, 2878.
[7] I. Vecchio, L. Sorrentino, A. Paoletti, R. Marra, M. Arbitrio, *J. Cent. Nerv. Sys. Dis.* **2021**, *13*, 117957352110291.
[8] A. Kaur, K. Nigam, I. Bhatnagar, H. Sukhpal, S. Awasthy, S. Shankar, A. Tyagi, S. Dang, *Drug Delivery Transl. Res.* **2020**, *10*, 1862.
[9] S. Al Harthi, S. E. Alavi, M. A. Radwan, M. M. El Khatib, I. A. AlSarra, *Sci. Rep.* **2019**, *9*, 1.
[10] G. Agraharam, N. Saravanan, A. Girigoswami, K. Girigoswami, *J. Bionanosci.* **2022**, *12*, 1.
[11] B. Begines, T. Ortiz, M. Pérez-Aranda, G. Martínez, M. Merinero, F. Argüelles-Arias, A. Alcudia, *Nanomaterials* **2020**, *10*, 1403.
[12] L. Del Amo, A. Cano, M. Ettcheto, E. B. Souto, M. Espina, A. Camins, M. L. García, E. Sánchez-López, *Appl. Sci.* **2021**, *11*, 4305.
[13] S. G. Jeon, M.-Y. Cha, J.-I. Kim, T. W. Hwang, K. A. Kim, T. H. Kim, K. C. Song, J.-J. Kim, M. Moon, *Nanomedicine* **2019**, *17*, 297.
[14] M. Yang, L. Jin, Z. Wu, Y. Xie, P. Zhang, Q. Wang, S. Yan, B. Chen, H. Liang, C. B. Naman, *J. Agric. Food Chem.* **2021**, *69*, 9764.
[15] D. Ege, *Materials* **2021**, *14*, 3332.
[16] A. Revdekar, P. Shende, *J. Controlled Release* **2021**, *340*, 271.
[17] Y. Xu, M. Zhao, D. Zhou, T. Zheng, H. Zhang, *Biomed. Pharmacother.* **2021**, *137*, 111360.
[18] J. Gupta, M. T. Fatima, Z. Islam, R. H. Khan, V. N. Uversky, P. Salahuddin, *Int. J. Biol. Macromol.* **2019**, *130*, 515.
[19] S. Hua, *Front. Pharmacol.* **2019**, *10*, 1328.
[20] A. Rezaei, A. Nasirpour, *J. Bionanosci.* **2019**, *9*, 438.
[21] K. AnjiReddy, S. Karpagam, *Int. J. Biol. Macromol.* **2019**, *124*, 871.
[22] M. Farokhi, F. Mottaghitalab, R. L. Reis, S. Ramakrishna, S. C. Kundu, *J. Controlled Release* **2020**, *321*, 324.
[23] H. Alenezi, M. E. Cam, M. Edirisinghe, *Appl. Phys. Rev.* **2019**, *6*, 041401.
[24] C. Işık, Y. İ. Doğaç, İ. Deveci, M. Teke, *ChemistrySelect* **2020**, *5*, 14380.
[25] N. Eghbalifam, S. A. Shojaosadati, S. Hashemi-Najafabadi, A. C. Khorasani, *Int. J. Biol. Macromol.* **2020**, *155*, 119.
[26] S. Abid, T. Hussain, Z. A. Raza, A. Nazir, *Mater. Sci. Eng., C* **2019**, *97*, 966.
[27] R. C. Feitosa, D. C. Geraldes, V. L. Beraldo-de-Araújo, J. S. R. Costa, L. Oliveira-Nascimento, *Front. Pharmacol.* **2019**, *10*, 1057.
[28] T. E. Böncü, N. Ozdemir, *Beilstein J. Nanotechnol.* **2022**, *13*, 245.
[29] S. M. D. Bhavna, M. Ali, S. Baboota, J. K. Sahni, A. Bhatnagar, J. Ali, *Drug Dev. Ind. Pharm.* **2014**, *40*, 278.
[30] I. Baysal, G. Ucar, M. Gultekinoglu, K. Ulubayram, S. Yabanoglu-Ciftci, *J. Neural Transm.* **2017**, *124*, 33.
[31] X. Tao, S. Mao, Q. Zhang, H. Yu, Y. Li, X. He, S. Yang, Z. Zhang, Z. Yi, Y. Song, *Nanoscale Res. Lett.* **2021**, *16*, 132.
[32] S. Rao, Y. Song, F. Peddie, A. M. Evans, *Int. J. Nanomed.* **2011**, *6*, 1245.
[33] S. Chavez, *One-step Coassembly of Nanocoatings and Effects of the Deposition Methods*, Doctoral Dissertations, University of Connecticut-Storrs **2020**. https://digitalcommons.lib.uconn.edu/dissertations/2504
[34] C. Drosou, M. Krokida, C. G. Biliaderis, *Food Hydrocolloids* **2018**, *77*, 726.
[35] H. Alenezi, M. E. Cam, M. Edirisinghe, *Appl. Phys. Rev.* **2021**, *8*, 041412.
[36] F. Yalcinkaya, B. Yalcinkaya, O. Jirsak, *J. Chromatogr. B Biomed. Appl.* **2016**, 67.
[37] M. A. Abureesh, A. A. Oladipo, M. Gazi, *Int. J. Biol. Macromol.* **2016**, *90*, 75.
[38] A. Kharazmi, N. Faraji, R. M. Hussin, E. Saion, W. M. M. Yunus, K. Behzad, *Beilstein J. Nanotechnol.* **2015**, *6*, 529.
[39] K. U. Khan, M. U. Minhas, M. Sohail, S. F. Badshah, O. Abdullah, S. Khan, A. Munir, M. Suhail, *Drug Dev. Ind. Pharm.* **2021**, *47*, 465.
[40] K. Barkat, M. Ahmad, M. U. Minhas, I. Khalid, A. Mahmood, *Polym. Bull.* **2021**, *78*, 5075.
[41] D. Poormoghadam, M. Ghollasi, H. Babavalian, A. Tabasi, M. Shams, V. Goodarzi, A. Salimi, *Mater. Lett.* **2021**, *300*, 130160.
[42] G. R. Topal, M. Mészáros, G. Porkolab, A. Szecskó, T. F. Polgár, L. Siklós, M. A. Deli, S. Veszelka, A. Bozkir, *Pharmaceutics* **2020**, *13*, 38.
[43] S. Cesur, M. E. Cam, F. S. Sayin, O. Gunduz, *J. Drug Deliv. Sci. Technol.* **2022**, *67*, 102977.
[44] P. Quan, W. Guo, D. Cun, M. Yang, *Int. J. Pharm.* **2023**, *632*, 122566.
[45] S. S. Shevade, M. T. Rustomjee, P. V. Devarajan, *AAPS PharmSciTech* **2023**, *24*, 61.
[46] S. B. Aziz, A. S. Marf, E. M. Dannoun, M. A. Brza, R. M. Abdullah, *Polymers* **2020**, *12*, 2184.
[47] M. Abdelhamied, A. Atta, A. Abdelreheem, A. Farag, M. El Okr, *J. Mater. Sci.: Mater. Electron.* **2020**, *31*, 22629.
[48] W. R. Rolim, J. C. Pieretti, D. L. Reno, B. A. Lima, M. H. Nascimento, F. N. Ambrosio, C. B. Lombello, M. Brocchi, A. C. S. de Souza, A. B. Seabra, *ACS Appl. Mater. Interfaces* **2019**, *11*, 6589.
[49] H. Lim, S. W. Hoag, *AAPS PharmSciTech* **2013**, *14*, 903.
[50] W. Guo, P. Quan, L. Fang, D. Cun, M. Yang, *Asian J. Pharm. Sci.* **2015**, *10*, 405.
[51] P. Zhang, L. Chen, W. Gu, Z. Xu, Y. Gao, Y. Li, *Biomaterials* **2007**, *28*, 1882.
[52] F. H. Falqi, O. A. Bin-Dahman, M. Hussain, M. A. Al-Harthi, *Int. J. Poly. Sci.* **2018**, *2018*, 1.
[53] M. S. Deepika, R. Thangam, T. S. Sheena, R. Vimala, S. Sivasubramanian, K. Jeganathan, R. Thirumurugan, *Mater. Sci. Eng., C* **2019**, *103*, 109716.
[54] K. Derakhshandeh, M. Erfan, S. Dadashzadeh, *Eur. J. Pharm. Biopharm.* **2007**, *66*, 34.
[55] D. Ç. Altındal, M. Gümüşderelioğlu, *J. Microencapsulation* **2016**, *33*, 53.
[56] L. P. Jahromi, M. Ghazali, H. Ashrafi, A. Azadi, *Heliyon* **2020**, *6*, e03451.
[57] L. P. Kolluru, S. A. Rizvi, M. D'Souza, M. J. D'Souza, *J. Drug Targeting* **2013**, *21*, 77.
[58] K. K. Rao, C.-S. Ha, *Polym. Bull.* **2009**, *62*, 867.
[59] T. Jamnongkan, S. Kaewpirom, *Kagoshima Daigaku Rigakubu Kiyo* **2010**, *1*, 43.
[60] S. Şenel, T. Comoglu, Taylor & Francis, **2018**, p. 23-431.
[61] M. M. Rawas-Qalaji, F. E. R. Simons, K. J. Simons, *Drug Dev. Ind. Pharm.* **2007**, *33*, 523.
[62] S. Bredenberg, M. Duberg, B. Lennernäs, H. Lennernäs, A. Pettersson, M. Westerberg, C. Nyström, *Eur. J. Pharm. Sci.* **2003**, *20*, 327.
[63] Z. Bayrak, C. Tas, U. Tasdemir, H. Erol, C. K. Ozkan, A. Savaser, Y. Ozkan, *Eur. J. Pharm. Biopharm.* **2011**, *78*, 499.

[64] N. Watcharadulyarat, M. Rattanatayarom, N. Ruangsawasdi, N. Patikarnmonthon, *Sci. Rep.* **2023**, *13*, 266.
[65] M. O. Alas, G. Dogan, M. S. Yalcin, S. Ozdemir, R. Genc, *ACS Omega* **2022**, *7*, 29967.
[66] L. M. de Medeiros, M. A. De Bastiani, E. P. Rico, P. Schonhofen, B. Pfaffenseller, B. Wollenhaupt-Aguiar, L. Grun, F. Barbé-Tuana, E. R. Zimmer, M. A. Castro, *Mol. Neurobiol.* **2019**, *56*, 7355.
[67] H.-R. Xie, L.-S. Hu, G.-Y. Li, *Chin. Med. J.* **2010**, *123*, 1086.
[68] A. Jämsä, K. Hasslund, R. F. Cowburn, A. Bäckström, M. Vasänge, *Biochem. Biophys. Res. Commun.* **2004**, *319*, 993.
[69] H. Zhang, Y. Zhao, M. Yu, Z. Zhao, P. Liu, H. Cheng, Y. Ji, Y. Jin, B. Sun, J. Zhou, *J. Controlled Release* **2019**, *296*, 14.
[70] H. Du, X. Liu, J. Xie, F. Ma, *ACS Chem. Neurosci.* **2019**, *10*, 2397.
[71] K. V. Krishna, R. N. Saha, S. K. Dubey, *ACS Chem. Neurosci.* **2020**, *11*, 4139.
[72] G. Marucci, M. Buccioni, D. D. Ben, C. Lambertucci, R. Volpini, F. Amenta, *Neuropharmacology* **2021**, *190*, 108352.
[73] Z.-R. Chen, J.-B. Huang, S.-L. Yang, F.-F. Hong, *Molecules* **2022**, *27*, 1816.
[74] D. Nunes, J. A. Loureiro, M. C. Pereira, *Pharmaceutics* **2022**, *14*, 2296.
[75] L. Duan, X. Li, R. Ji, Z. Hao, M. Kong, X. Wen, F. Guan, S. Ma, *Polymers (Basel)* **2023**, *15*, 2196.
[76] M. Doğan, F. Gurgah, *J. Res. Pharm.* **2022**, *26*.
[77] M. E. Cam, B. Ertas, H. Alenezi, A. N. Hazar-Yavuz, S. Cesur, G. S. Ozcan, C. Ekentok, E. Guler, C. Katsakouli, Z. Demirbas, *Mater. Sci. Eng., C* **2021**, *119*, 111586.
[78] E. Guler, Y. E. Baripoglu, H. Alenezi, A. Arikan, R. Babazade, S. Unal, G. Duruksu, F. S. Alfares, Y. Yazir, F. N. Oktar, *Int. J. Biol. Macromol.* **2021**, *190*, 244.
[79] S. Erzengin, E. Guler, E. Eser, E. B. Polat, O. Gunduz, M. E. Cam, *Int. J. Biol. Macromol.* **2022**, *204*, 429.
[80] F. Sharif, S. Tabassum, W. Mustafa, A. Asif, F. Zarif, M. Tariq, S. A. Siddiqui, M. A. Gilani, I. Ur Rehman, S. MacNeil, *Polym. Compos.* **2019**, *40*, 1564.
[81] C. Capitini, A. Bigi, N. Parenti, M. Emanuele, N. Bianchi, R. Cascella, C. Cecchi, L. Maggi, F. Annunziato, F. S. Pavone, M. Calamai, *iScience* **2023**, *26*, 106611.

